

X-ray Sources

Thomas Andrade Hernández*
PhD. Carlos Ávila Bernal**

- ▶ About 12% of women worldwide are at risk of developing breast cancer¹.
- ▶ Clinical experience remains the most important factor for a reliable diagnosis.

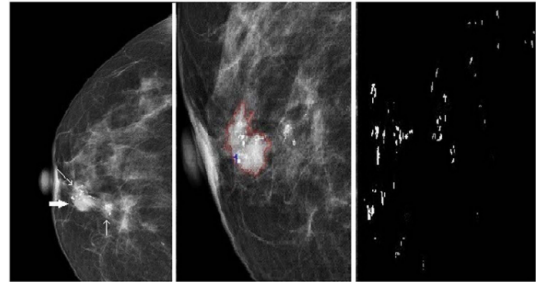


Figure 1: Mammography image example with microcalcifications. Image from [2].

¹N. Fico et al., "Breast imaging physics in mammography (part i)," vol. 13, no. 20, 2023. doi: 10.3390/diagnostics13203227

²J. Wang et al., "Discrimination of breast cancer with microcalcifications on mammography by deep learning," *Scientific Reports*, vol. 6, p. 27327, Jun. 2016. doi: 10.1038/srep27327

XPCI exploits a property different from the well-known attenuation³; this property refers to the **phase**. To understand it, we introduce the concept of a **complex refractive index**:

$$n = 1 - \delta + i\beta \quad (1)$$

Here, β represents the attenuation effects, while δ accounts for the phase effects⁴. In soft tissue, this difference is about three orders of magnitude.

³F Arfelli et al., "Low-dose phase contrast x-ray medical imaging," , vol. 43, no. 10, pp. 2845–2852, Oct. 1, 1998. doi: 10.1088/0031-9155/43/10/013

⁴M. Endrizzi, "X-ray phase-contrast imaging," , Radiation Imaging Techniques and Applications, vol. 878, pp. 88–98, Jan. 11, 2018. doi: 10.1016/j.nima.2017.07.036

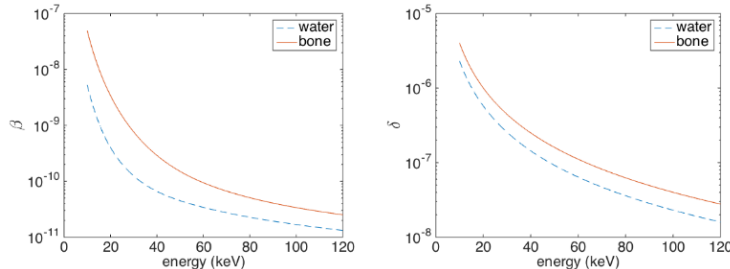


Figure 2: Complex index of refraction for water and bone as a function of X-ray energy. Image from [4].

⁴M. Endrizzi, "X-ray phase-contrast imaging," *Radiation Imaging Techniques and Applications*, vol. 878, pp. 88–98, Jan. 11, 2018. doi: 10.1016/j.nima.2017.07.036

Dark-field imaging captures ultrasmall-angle X-ray scattering caused by microstructural inhomogeneities smaller than the system resolution. It is particularly sensitive to features such as fibers, pores, or fine tissue structures, producing strong signals in samples like composite materials, bone, and lung.

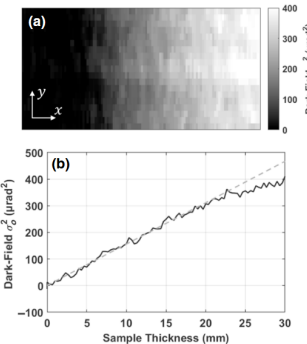


Figure 3: Dark field measurements of an inhomogeneous wedge that gets thicker as moving to the right. Image from [5].

⁵A. Doherty et al., “Edge-illumination x-ray dark-field tomography,”, vol. 19, p. 054 042, 5 2023. doi: 10.1103/PhysRevApplied.19.054042



Most XPCI methods require at least one of the following conditions to be properly implemented⁶:

1. Considerable beam coherence, being achieved by a synchrotron source or considerable big source to detector distance. (**Propagation Based, Grating Based Interferometry**)
2. Detectors with high resolution. (**Analyzer Based Interferometry**)
3. Microtube X-ray sources with focal spots of $\approx 10\mu\text{m}$.

⁶ A. Zamir et al., "Recent advances in edge illumination x-ray phase-contrast tomography," vol. 4, no. 4, p. 040901, Oct. 2017. doi: 10.1117/1.JMI.4.4.040901

This method is characterized by the presence of **two masks**: one creates fringes, while the other selectively filters them.

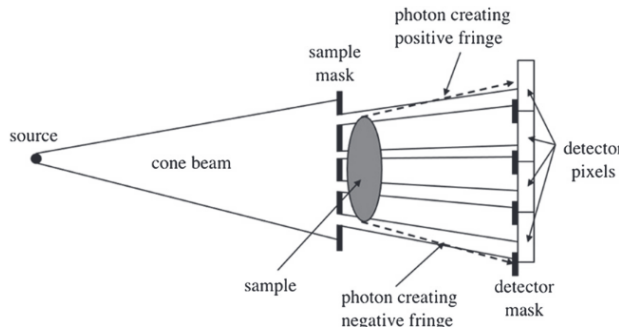


Figure 4: Conventional edge illumination setup. Image from [7].

⁷ A. Olivo, "Edge-illumination x-ray phase-contrast imaging," vol. 33, no. 36, p. 363 002, Jul. 2021, Publisher: IOP Publishing. doi: 10.1088/1361-648X/ac0e6e

Edge illumination can be achieved by using only **one mask** positioned to illuminate a specific region between pixels.

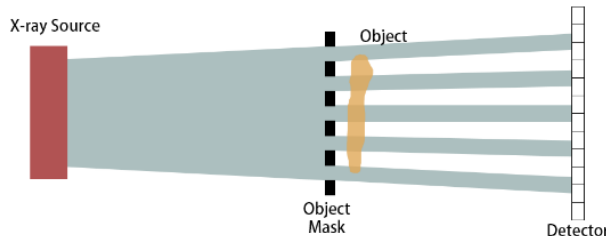


Figure 5: Single mask modality of the edge illumination setup. Image from [8].

⁸J. Yuan and I. Harmon, "Comparing SNR benefits between single-mask edge-illumination and free-space propagation x-ray phase contrast imaging,"

Study the feasibility of implementing XPCI with Edge Illumination in the single-mask modality for clinical X-ray setups.

Specific Objectives:

- ▶ Identify the key setup parameters required for effective Edge Illumination (EI).
- ▶ Develop an open-source code for phase retrieval using EI.
- ▶ Perform computational simulations with PEPI to evaluate spatial resolution and contrast for various clinical X-ray setups.
- ▶ Conduct experimental studies with clinical setups and medical phantoms to validate the computational results.

Astolfo et al.⁹ investigated how the focal spot size influences phase retrieval and dark-field measurements. They found that all signal values remained consistent across different effective focal spot sizes, except for scatter, which showed a slight increase with larger focal spots.

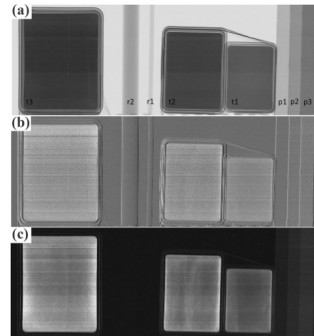


Figure 6: Measurements of attenuation, phase and dark field of a phantom. Image from [9]

⁹ A. Astolfo et al., "The effect of a variable focal spot size on the contrast channels retrieved in edge-illumination x-ray phase contrast imaging.", vol. 12, no. 1, p. 3354, Mar. 1, 2022, Publisher: Nature Publishing Group. doi: 10.1038/s41598-022-07376-0

Jingchuang Yuan and Mini Das¹⁰ proposed a method for simultaneous **phase contrast** and **dark-field** imaging. Their approach is based on the **Transport of Intensity Equation** (TIE):

$$I(z, \vec{r}) = I(0, \vec{r}) - \frac{z}{k} \left(\nabla_{\perp} I(0, \vec{r}) \cdot \nabla_{\perp} \phi(\vec{r}) + I(0, \vec{r}) \nabla_{\perp}^2 \phi(\vec{r}) \right) \quad (2)$$

In the Propagation-Based formulation, the first term is said to be negligible ($\nabla_{\perp} I(0, \vec{r}) \cdot \nabla_{\perp} \phi(\vec{r}) \approx 0$), so that:

$$I(z, \vec{r}) = I(0, \vec{r}) - \frac{z}{k} I(0, \vec{r}) \nabla_{\perp}^2 \phi(\vec{r}) \quad (3)$$

¹⁰J. Yuan and M. Das, *Single-shot, single-mask x-ray dark-field and phase contrast imaging*, Jun. 3, 2025. doi: 10.48550/arXiv.2506.02427 arXiv: 2506.02427 [physics]. Accessed: Sep. 16, 2025

For the mask case, the assumption of minimal variation no longer holds, so the first term cannot be neglected. Assuming $I(z, \vec{r}) = T(\vec{r})M(x)$:

$$\nabla_{\perp} I(0, \vec{r}) = T \nabla_{\perp} M + M \nabla_{\perp} T \approx T \partial_x M \quad (4)$$

The TIE then becomes, after integration over the pixel regions:

$$I_n = \int_{x_n}^{x_{n+1}} T \cdot M \, dx - \frac{z}{k} \int_{x_n}^{x_{n+1}} T \cdot \partial_x M \cdot \partial_x \phi \, dx - \frac{z}{k} \int_{x_n}^{x_{n+1}} T \cdot M \cdot \nabla_{\perp}^2 \phi \, dx \quad (5)$$

Finally, assuming $M(x)$ is a square-wave function with coefficients C_m depending on the mask properties¹¹:

$$M(x) = \sum_m C_m \cos\left(\frac{2\pi mx}{2\rho}\right) \quad (6)$$

¹¹ J. Yuan and M. Das, "Transport-of-intensity model for single-mask x-ray differential phase contrast imaging," vol. 11, no. 4, p. 478, Apr. 20, 2024.
 DOI: 10.1364/OPTICA.510537 Accessed: Apr. 18, 2025

The case of only phase retrieval ends up being:

$$T_n(1 - L_n) \approx \frac{\bar{I}_n + \bar{I}_{n+1}}{2} \quad (7)$$

$$\frac{\alpha}{w_e} D_n \approx \frac{\bar{I}_n - \bar{I}_{n+1}}{\bar{I}_n + \bar{I}_{n+1}} (-1)^n \quad (8)$$

Here $\bar{I}_n = I_n^{(S)} / I_n^{(M)}$. $I_n^{(S)}$ are the intensities of the image with de mask and object, while $I_n^{(M)}$ the ones with only the mask.

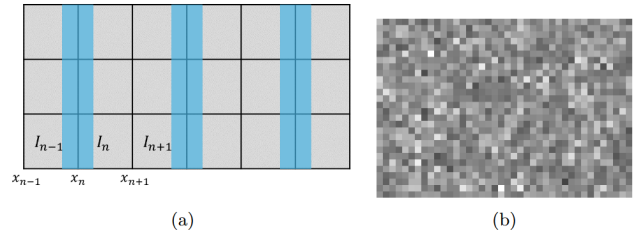


Figure 7: Required setup for the phase contrast map acquisition. Image from [10].

¹⁰J. Yuan and M. Das, *Single-shot, single-mask x-ray dark-field and phase contrast imaging*, Jun. 3, 2025. doi: 10.48550/arXiv.2506.02427 arXiv: 2506.02427 [physics]. Accessed: Sep. 16, 2025

For dark-field-only retrieval, the equations become:

$$T_n(1 - L_n) = \frac{I_n^{(S)} + I_{n+1}^{(S)}}{I_n^{(M)} + I_{n+1}^{(M)}} \quad (9)$$

$$\frac{\alpha_3}{\alpha_1} S_n = 1 - \frac{I_n^{(S)} - I_{n+1}^{(S)}}{I_n^{(M)} - I_{n+1}^{(M)}} \cdot \frac{I_n^{(M)} + I_{n+1}^{(M)}}{I_n^{(S)} + I_{n+1}^{(S)}} \quad (10)$$

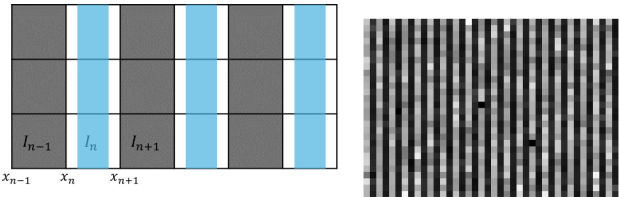


Figure 8: Required setup for the dark-field acquisition. Image from [10].

¹⁰J. Yuan and M. Das, *Single-shot, single-mask x-ray dark-field and phase contrast imaging*, Jun. 3, 2025. doi: 10.48550/arXiv.2506.02427 arXiv: 2506.02427 [physics]. Accessed: Sep. 16, 2025

For simultaneous retrieval, the equations are:

$$T_n(1 - L_n) = \frac{I_{n-1}^{(S)} + I_n^{(S)} + I_{n+1}^{(S)}}{I_{n-1}^{(M)} + I_n^{(M)} + I_{n+1}^{(M)}} \quad (11)$$

$$\frac{2\alpha_2}{w_e + \frac{1}{2}\alpha_1} D_n = \left(\frac{I_{n-1}^{(S)}}{I_{n-1}^{(M)}} - \frac{I_n^{(S)}}{I_n^{(M)}} \right) \frac{I_{n-1}^{(M)} + I_n^{(M)} + I_{n+1}^{(M)}}{I_{n-1}^{(S)} + I_n^{(S)} + I_{n+1}^{(S)}} \quad (12)$$

$$\frac{2\alpha_3}{w_e + 2\alpha_1} S_n = \left[1 - \frac{I_{n-1}^{(S)} + I_n^{(S)} - I_{n+1}^{(S)}}{I_{n-1}^{(M)} + I_n^{(M)} - I_{n+1}^{(M)}} \frac{I_{n-1}^{(M)} + I_n^{(M)} + I_{n+1}^{(M)}}{I_{n-1}^{(S)} + I_n^{(S)} + I_{n+1}^{(S)}} \right] \quad (13)$$

Here, T_n , D_n , and S_n correspond to the transmission, differential phase, and dark-field signals, respectively.

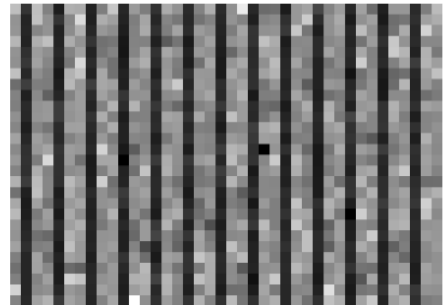
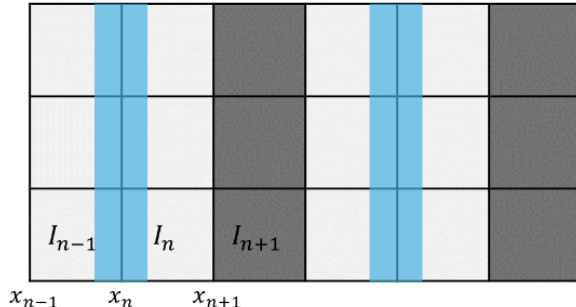


Figure 9: Required setup for the simultaneous acquisition. Image from [10].

¹⁰J. Yuan and M. Das, *Single-shot, single-mask x-ray dark-field and phase contrast imaging*, Jun. 3, 2025. doi: 10.48550/arXiv.2506.02427 arXiv: 2506.02427[physics]. Accessed: Sep. 16, 2025

Simulation Framework

This project uses the Geant4 framework developed at CERN, which has been adapted for phase-contrast imaging simulations¹². Additionally, Luca Brombal at the University of Trieste has released an open-access code called Photon-counting Edge-illumination Phase-contrast Imaging (PEPI)¹³.

¹²L. Brombal et al., "A geant4 tool for edge-illumination x-ray phase-contrast imaging," *J. Inst.*, vol. 17, no. 1, p. C01043, Jan. 2022, Publisher: IOP Publishing. doi: 10.1088/1748-0221/17/01/C01043

¹³L. Brombal et al., "PEPI lab: A flexible compact multi-modal setup for x-ray phase-contrast and spectral imaging," , vol. 13, no. 1, p. 4206, Mar. 14, 2023, Publisher: Nature Publishing Group. doi: 10.1038/s41598-023-30316-5 Accessed: Mar. 30, 2025

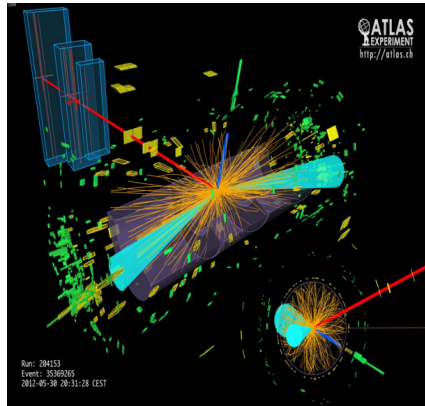


Figure 10: Image of the ATLAS detector at CERN simulated using Geant4. Image taken from the ATLAS official website.

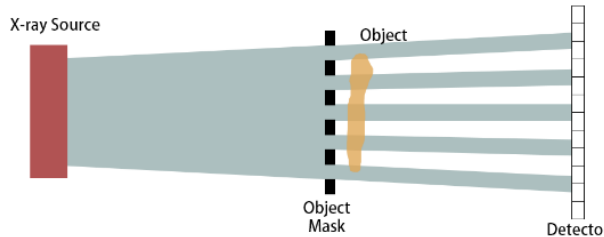


Figure 11: Single mask modality of the edge illumination setup. Image from [8].

⁸J. Yuan and I. Harmon, "Comparing SNR benefits between single-mask edge-illumination and free-space propagation x-ray phase contrast imaging,"

Simulation Parameters

The following parameters were considered throughout the simulations:

1. Source-to-detector distance: 70 cm.
2. Mask-to-detector distances: 50 cm, 46 cm, 42 cm, ..., 18 cm, 14 cm, 10 cm.
3. Focal spot sizes: 10 μm , 100 μm , 200 μm , and 300 μm .

The chosen configuration follows the study by Fico et al.¹, which describes the characteristics of the mammography setup.

¹N. Fico et al., "Breast imaging physics in mammography (part i)," vol. 13, no. 20, 2023. doi: 10.3390/diagnostics13203227



- ▶ For each distance, a simulation with 1×10^6 events was performed. The X-ray beam was projected onto a detector of 1024×1024 pixels, each with a size of $10\mu\text{m}$.

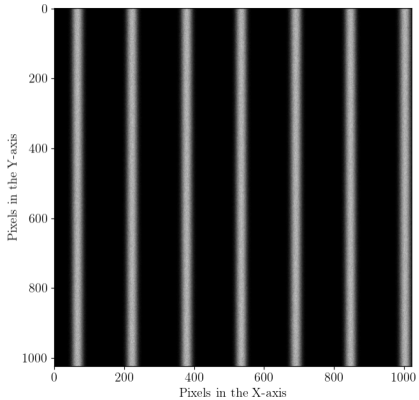
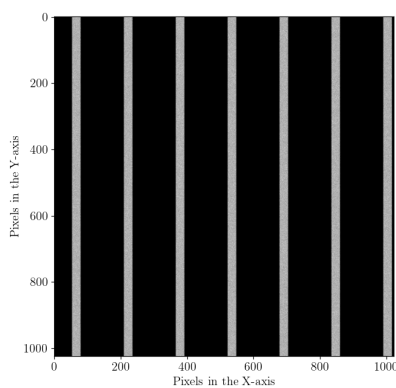


Figure 12: From left to right: measurements with 10 μm and 100 μm focal spots. Same measurement setup: mask-to-detector distance 46 cm, mask aperture 90 μm .

- ▶ The intensity was projected along the x-axis, and only measurements exceeding a threshold of 5% of the maximum intensity were considered.

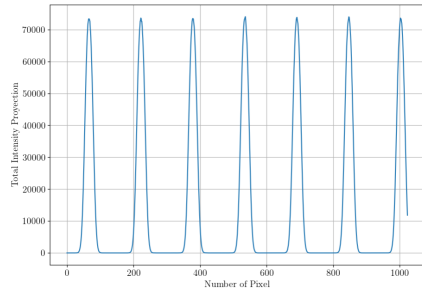
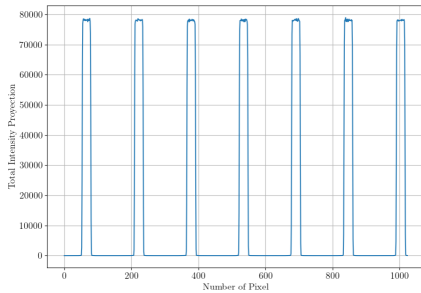


Figure 13: From left to right: measurements with 10 μm and 100 μm focal spots. Same measurement setup: mask-to-detector distance 46 cm, mask aperture 90 μm .

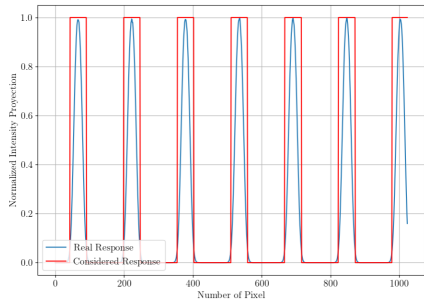
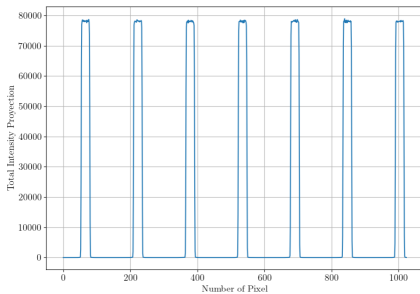


Figure 14: From left to right: measurements with $10\text{ }\mu\text{m}$ and $100\text{ }\mu\text{m}$ focal spots. Same measurement setup: mask-to-detector distance 46 cm, mask aperture $90\text{ }\mu\text{m}$.

- ▶ The mask aperture size was then varied to study how the beams are magnified, repeating the procedure for multiple distances.

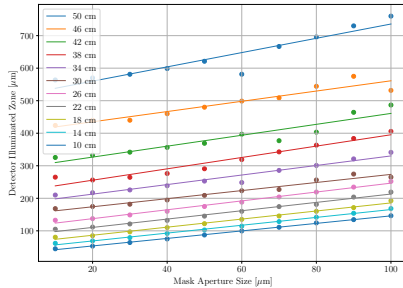
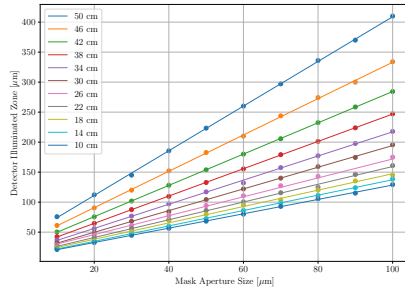


Figure 15: From left to right: measurements with 10 μm and 100 μm focal spots. Same measurement setup: mask-to-detector distance 46 cm, mask aperture 90 μm .

These magnifications were measured and show a trend that can be explained using the geometric magnification formula of a cone-beam source¹⁴:

$$p_{\text{detector}} = M p_{\text{mask}} = \frac{d_{SD}}{d_{SM}} p_{\text{mask}} = \frac{d_{SD}}{d_{SD} - d_{MD}} p_{\text{mask}}$$

$$\frac{p_{\text{detector}}}{p_{\text{mask}}} = \frac{1}{1 - \frac{d_{MD}}{d_{SD}}} = M(d_{MD}, d_{SD})$$

For a non-ideal scenario, the formula can be generalized as:

$$M(d_{MD}, d_{SD}, FS, E) = \frac{1}{1 - \frac{d_{MD}}{\alpha(d_{SD}, FS, E)}} \quad (14)$$

¹⁴D. M. Paganin and D. Pelliccia, "X-ray phase-contrast imaging: A broad overview of some fundamentals," in vol. 218, 2021, pp. 63–158. arXiv: 2011.05146 [eess]

The $M(d_{MD}, d_{SD}, FS, E)$ can be visualized as follows:

$$\delta = \frac{M + 1}{2} p_{mask} \quad (15)$$

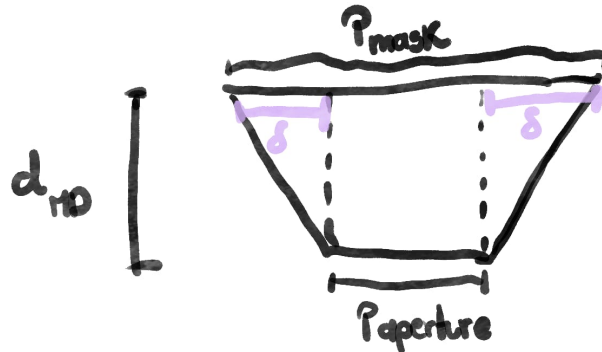


Figure 16: Sketch of what I mean.

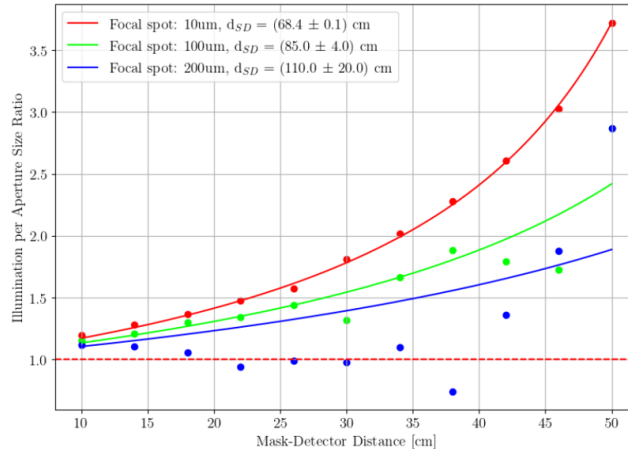


Figure 17: Magnification of the beamlet as a function of the mask-detector distance for several focal spots.

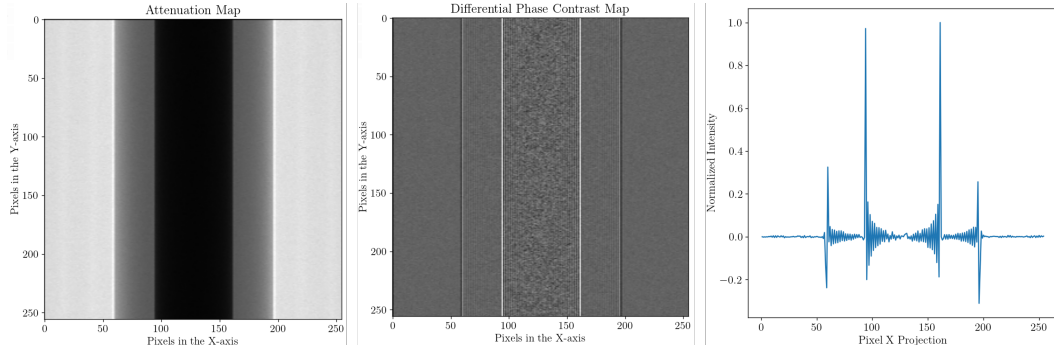


Figure 18: Ideal scenario only phase retrieval.

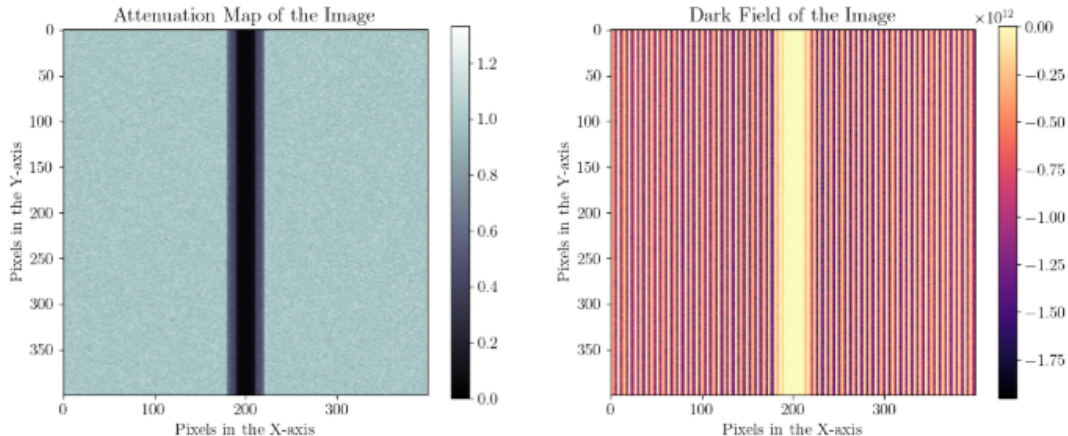


Figure 19: Non ideal scenario only dark field.

The overall progress of the project has been:

- ▶ Identify the key setup parameters required for effective Edge Illumination (EI) (70%).
- ▶ Develop an open-source code for phase retrieval using EI (100%).
- ▶ Perform computational simulations with PEPI to evaluate spatial resolution and contrast for various clinical X-ray setups (20%).
- ▶ Conduct experimental studies with clinical setups and medical phantoms to validate the computational results (0%).

- ▶ Need to closely observe the behavior for 200 μm and 300 μm focal spots, which appear unusual.
- ▶ Once these cases are analyzed, proceed to examine other scenarios for large focal spots (Yuan & Das).
- ▶ Assess how the CNR and SNR change for the same setup with different focal spot sizes.

- ▶ What is the equivalence between the simulated events and the radiation dose received by a person? (Try to estimate.)
- ▶ What happens if the X-ray source energy is increased?
- ▶ What results do you expect based on the current simulations?

- [1] N. Fico et al., "Breast imaging physics in mammography (part i)," , vol. 13, no. 20, 2023. doi: 10.3390/diagnostics13203227
- [2] J. Wang, X. Yang, H. Cai, W. Tan, C. Jin, and L. Li, "Discrimination of breast cancer with microcalcifications on mammography by deep learning," *Scientific Reports*, vol. 6, p. 27327, Jun. 2016. doi: 10.1038/srep27327
- [3] F Arfelli et al., "Low-dose phase contrast x-ray medical imaging," , vol. 43, no. 10, pp. 2845–2852, Oct. 1, 1998. doi: 10.1088/0031-9155/43/10/013
- [4] M. Endrizzi, "X-ray phase-contrast imaging," , *Radiation Imaging Techniques and Applications*, vol. 878, pp. 88–98, Jan. 11, 2018. doi: 10.1016/j.nima.2017.07.036
- [5] A. Doherty, S. Savvidis, C. Navarrete-León, M. F. Gerli, A. Olivo, and M. Endrizzi, "Edge-illumination x-ray dark-field tomography," , vol. 19, p. 054042, 5 2023. doi: 10.1103/PhysRevApplied.19.054042

- [6] A. Zamir et al., "Recent advances in edge illumination x-ray phase-contrast tomography," *vol. 4, no. 4, p. 040901, Oct. 2017.* doi: [10.1117/1.JMI.4.4.040901](https://doi.org/10.1117/1.JMI.4.4.040901)
- [7] A. Olivo, "Edge-illumination x-ray phase-contrast imaging," *vol. 33, no. 36, p. 363002, Jul. 2021,* Publisher: IOP Publishing. doi: [10.1088/1361-648X/ac0e6e](https://doi.org/10.1088/1361-648X/ac0e6e)
- [8] J. Yuan and I. Harmon, "Comparing SNR benefits between single-mask edge-illumination and free-space propagation x-ray phase contrast imaging,"
- [9] A. Astolfo et al., "The effect of a variable focal spot size on the contrast channels retrieved in edge-illumination x-ray phase contrast imaging," *vol. 12, no. 1, p. 3354, Mar. 1, 2022,* Publisher: Nature Publishing Group. doi: [10.1038/s41598-022-07376-0](https://doi.org/10.1038/s41598-022-07376-0)

- [10] J. Yuan and M. Das, *Single-shot, single-mask x-ray dark-field and phase contrast imaging*, Jun. 3, 2025. doi: 10.48550/arXiv.2506.02427 arXiv: 2506.02427 [physics]. Accessed: Sep. 16, 2025.
- [11] J. Yuan and M. Das, “Transport-of-intensity model for single-mask x-ray differential phase contrast imaging,”, vol. 11, no. 4, p. 478, Apr. 20, 2024. doi: 10.1364/OPTICA.510537 Accessed: Apr. 18, 2025.
- [12] L. Brombal, L. Rigon, F. Arfelli, R. Menk, and F. Brun, “A geant4 tool for edge-illumination x-ray phase-contrast imaging,” *J. Inst.*, vol. 17, no. 1, p. C01043, Jan. 2022, Publisher: IOP Publishing. doi: 10.1088/1748-0221/17/01/C01043

- [13] L. Brombal, F. Arfelli, R. H. Menk, L. Rigon, and F. Brun, “PEPI lab: A flexible compact multi-modal setup for x-ray phase-contrast and spectral imaging,” vol. 13, no. 1, p. 4206, Mar. 14, 2023, Publisher: Nature Publishing Group. doi: 10.1038/s41598-023-30316-5 Accessed: Mar. 30, 2025.
- [14] D. M. Paganin and D. Pelliccia, “X-ray phase-contrast imaging: A broad overview of some fundamentals,” in vol. 218, 2021, pp. 63–158. arXiv: 2011.05146 [eess].